Journal Name

Controlling the Emission in Flexibly-Linked (N^C^N)Platinum Dyads

Received 00th January 20xx,
Accepted 00th January 20xx

DOI: 10.1039/x0xx00000x

www.rsc.org/

Eleonora Garoni,[a,b] Julien Boixel,[a] Vincent Dorcet,[a] Thierry Roisnel,[a] Dominique Roberto,[b] Denis Jacquemin*[c,d] and Véronique Guerchais*[a]

The synthesis, spectroscopic and theoretical characterizations of dinuclear Pt(II) complexes where the two chromophoric units are connected though a polyether chain via either the central benzene ring of the tridentate ligand dpyb (**Pt-2**), or the phenylacetylide ligand (**Pt-3**), are described. The spacer, which contains four oxyethylene -CH_2CH_2O- units, is flexible and long enough to allow a self-association of the Pt units by folding, as shown by DFT calculations. Comparison of the photophysical properties of the dinuclear complex **Pt-2** with those of the mononuclear complex **Pt-1**, used as reference, demonstrates the key role played by the linker group in the interaction processes. In addition, the emission of complex **Pt-2** was found to be affected by the temperature, nature of the solvent, and cation coordination as evidenced by luminescence and ^{1}H NMR studies. The interacting processes are highly dependent on the solvent polarity that controls the - extended *vs* folded- arrangement and, consequently, induces solvatochromic shifts. This unique photophysical behavior of **Pt-2** allows the modulation of the emission from green to deep-red (up to 125 nm) over the visible part of the spectrum. By contrast, complex **Pt-3** has a high propensity to form a red-shifted intense emissive excimer. DFT and TD-DFT investigations of the excimers in **Pt-2** and **Pt-3** consistently show a much stronger interaction in the latter complex.

Introduction

Inorganic complexes displaying strong luminescence can be built using many transition metals, and, among them, square planar Pt(II) complexes with terdentate coordinating ligands display particularly interesting photophysical properties and have found applications in opto-electronics devices.[1-3] Importantly, their square planar geometry favours intermolecular interactions, that is π···π and Pt···Pt interactions, in both concentrated solution and in solid state allowing the formation of aggregates and the appearance of excimers.[2-4] These specific self-assembly properties have been used for the development of molecular probes, as well as for the elaboration of well-defined nanostructures.[5,6] In this context, several dinuclear platinum complexes in which the two organometallic moieties are linked through a flexible or rigid bridge have been developed in order to obtain intense deep red and near infrared emitters, taking advantage of their specific interactions.[7]

The study of the photophysics of square-planar Pt(N^C^N)Cl complexes containing a 1,3-di(2-pyridyl)benzene (dpyb) ligand was initiated by Williams and co-workers, who demonstrated that an intense phosphorescence resulted from cyclometallation which effectively suppresses the non-radiative *d-d* deactivation pathway.[8] The large emission quantum yields accompanying the possible fine–tuning of the emission wavelength by facile ligand modification makes this class of organometallic luminophores particularly attractive.[9] Furthermore, their propensity to form excimers has been successfully exploited for the fabrication of white light-emitting OLEDs (WOLEDs).[10] Within the series of (dpyb)Pt complexes, the rigidly-linked diplatinum complex xant-$(dpybPtCl)_2$, in which a 4,5-disubstitued xanthene unit locks the two metal units into a face-to-face configuration, has been shown to be very efficient in promoting the formation of *intramolecular* excimers (Scheme 1).[11] However, to the very best of our knowledge, the corresponding *flexibly*-linked diplatinum complexes were not investigated to date and we focus on this unexplored class here. We reasoned that the presence of a flexible bridge could favour intramolecular

[a] *Institut des Sciences Chimiques de Rennes UMR CNRS 6226,Université de Rennes 1, Campus de Beaulieu, 35042 Rennes Cedex (France) E-mail: Veronique.Guerchais@univ-rennes1.fr*
[b] *Dipartimento di Chimica Università degli Studi di Milano,via Golgi 19, 20133 Milano (Italy)*
[c] *CEISAM laboratory UMR 6230, University of Nantes, 2, rue de la Houssinière44322 Nantes (France). E-mail: Denis.Jacquemin@univ-nantes.fr*
[d] *Institut Universitaire de France, 1, rue Descartes, 75231 Paris Cedex 05 (France)*

† Electronic Supplementary Information (ESI) available: NMR spectra for all new compounds (Figures S1-S11), details of X-ray structure determination, crystallographic data collection parameters for **Pt-1** are listed in Table S1. Additional photophysical data (Figures S12-S22 and Table S2). Details of the DFT and TD-DFT calculations, additional theoretical data (Figures S23-26 and Table S3). See DOI: 10.1039/x0xx00000x.

association, *i.e.*, a folded state that is likely to favour Pt···Pt and π···π interactions and consequently impact on the luminescence properties.

Herein, we describe the synthesis, spectroscopic and theoretical characterizations of two different dinuclear Pt(II) complexes where the two Pt units are connected through a polyether bridge via either the central benzene ring of the tridentate ligand dpyb (**Pt-2**), or the phenylacetylide ligand (**Pt-3**) that are displayed in Scheme 1. For both compounds, we show that the flexible spacer, a four oxyethylene -CH_2CH_2O chain, favours intramolecular interacting processes between the two adjacent chromophoric units. We describe below the unique luminescence properties of the dinuclear complex **Pt-2** and compare them to, one the one hand, those of the momonuclear complex **Pt-1**[12] (Scheme 1) which was used as a reference to quantify the role of the linker group in the interaction processes, and, on the other hand those of the bis-alkynyl diplatinum complex **Pt-3** featuring a different design. We demonstrate that this class of charge-neutral (dpyb)-based complexes displays a unique behaviour, very different from that of Pt (II) complexes containing terdentate (N^N^N) ligands that are subject to ground state aggregation properties giving rise to metal-metal-to-ligand charge transfer (MMLCT) transitions characterized by a low-energy band in the electronic absorption spectra.[2-7,12] We envisioned that complex **Pt-2** can possibly exhibit different arrangements (see Chart 1): the extended form **a** (Scheme 1) that should simply behave as the sum of two independent **Pt-1** units, the *intra*molecular face-to-face conformation **b**, and the *inter*molecular head-to-tail association **c**, such head-to-tail arrangement being impossible *intra*molecularly as the linker is too short. In both **b** and **c** the changes in the interactions between the two Pt units are expected to give rise to different spectral emission profiles.

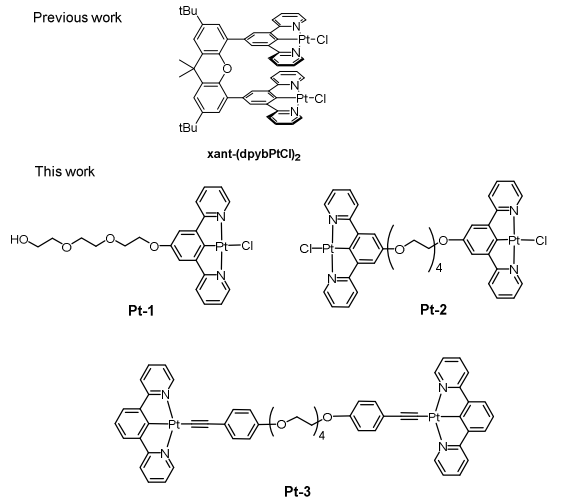

Scheme 1 Chemical structures of xant-(dpybPtCl)$_2$, and the mono- (**Pt-1**), and dinuclear Pt(II) complexes **Pt-2** and **Pt-3** in their extended forms (**a**).

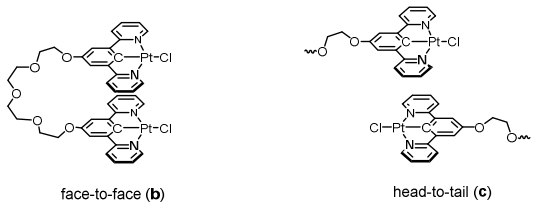

Chart 1 Proposed intra- (**b**) and intermolecular (**c**) arrangements of **Pt-2**.

As we detail below, the self-association of dinuclear complex **Pt-2** was found to be dependent on the temperature, polarity of solvent, and cation binding as evidenced by luminescence and ^{1}H NMR studies, allowing a modulation of the emission over a large range (up to 125 nm) of the visible spectrum. We also present the higher propensity of **Pt-3,** compared to **Pt-2**, to form a red-shifted intense emissive excimer. First principle characterizations of the ground and lowest triplet excited states of the different conformers of the complexes further support the interpretations. In short, the present joint experimental and theoretical study therefore provides insights into the interaction processes and demonstrates the beneficial effect of the flexible linker that allows the formation of the excimer in dinuclear (N^C^N-dpyb) complexes in spite of the influence of the electron-donating alkoxy group, that plays a detrimental role in the mononuclear **Pt-1**.

Experimental

General comments

All reactions were performed using standard Schlenk techniques under inert (Ar) atmosphere with reagent-grade solvents. Freshly distilled anhydrous THF was used and toluene was obtained from a SPS-800 M-Braun solvent purification system. Flash column chromatography was performed using silica gel (Silica-P from Silicycle, 60 Å, 40-63 µm). Commercially available chemicals: tetraethylene glycol, 4-toluensulphonyl chloride, 3,5-dibromophenol and catalysts $Pd(PPh_3)_4$ and $Pd(Ph_3)_2Cl_2$ were used as supply. Compound **1** was synthesized following a reported procedure,[13] from the commercially available 3,5-dibromophenol and tetraethylene glycol ditosylate.[14] 2-(tributylstannyl)pyridine and Pt(di(2-pyridylbenzene)Cl were prepared according to the literature[8] 1,2-bis(4-ethynylphenoxy)ethane[7a] were prepared as reported. ^{1}H and ^{13}C solution-NMR spectra were recorded on a Bruker, AV 400 spectrometer. ^{1}H NMR spectra were referenced to the solvent peak. High resolution mass spectra (HRMS) were recorded on a MS/MS ZABSpec TOF at the CRMPO (*Centre de Mesures Physiques de l'Ouest*) in Rennes. Elemental analyses were performed at the CRMPO.

Synthesis and isolation of the compounds

Synthesis of 1. To a solution of 3,5-dibromophenol (1.00 g, 2 mmol) in 40 mL of acetonitrile, tetraethylene glycol ditosylate (1.00 g, 4 mmol) and anhydrous K_2CO_3 (825 mg, 6 mmol) were added. The reaction mixture was refluxed under argon atmosphere for 12 hours. After cooling to room temperature,

the resulting suspension was extracted with water and dichloromethane (3 x 40 mL). The organic layer was dried over $MgSO_4$ and concentrated in *vacuo*. Compound **1** was obtained as an orange oil (1.32 g). Yield: 99%. ^{1}H NMR (400 MHz, $CDCl_3$) δ (ppm): 7.23 (s, 2H, H_{Ar}), 7.00 (s, , 4H, H_{Ar}), 4.08 (t, *J* = 4.6 Hz, 4H, H_α), 3.82 (t, *J* = 4.5 Hz, 4H, H_β), 3.67 (m, 8H, $H_{\gamma,\delta}$). ^{13}C NMR (100 MHz, $CDCl_3$) δ (ppm): 159.9, 126.6, 123.0, 117.1, 70.9, 70.7, 69.4, 68.1. Elem. Anal. Calcd for $C_{20}H_{22}Br_4O_5$: C, 36.29; H, 3.35. Found: C, 36.85; H, 3.48.

Synthesis of 2. A mixture of **1** (827 mg, 1.3 mmol), 2-(tri-*n*-butylstannyl)pyridine (3.68 g, 10.0 mmol), $PdCl_2(PPh_3)_2$ (84 mg, 0.1 mmol) and LiCl (954 mg, 22.5 mmol) was suspended in toluene (12 mL) and heated at reflux under argon atmosphere for 48 hours. After cooling to room temperature, an aqueous solution of NaOH 1 M (30 mL) was added. The resulting solution was extracted with AcOEt (3 x 60 mL) and the organic layer was dried over $MgSO_4$ and evaporated in *vacuo*. The crude product was purified by column chromatography (silica, from AcOEt to AcOEt/MeOH, 96:4) to obtain **2** as a white solid (379 mg). Yield: 46%. ^{1}H NMR (400 MHz, $CDCl_3$) δ (ppm): 8.68 (d, *J* = 4.8 Hz, 4H, H_6), 8.20 (s, 2H, $H_{4'}$), 7.81 (d, *J* = 8.0 Hz, 4H, H_3), 7.73 (dt, *J* = 7.5 Hz, 1.8 Hz, 4H, H_4), 7.66 (s, 4H, $H_{2'}$), 7.23 (ddd, *J* = 7.4, 4.8, 1.2 Hz, 4H, H_5), 4.33 (t, *J* = 4.8 Hz, 4H, H_α), 3.91 (t, *J* = 5.2 Hz, 4H, H_β), 3.73 (m, 8H, $H_{\gamma,\delta}$). ^{13}C NMR (100 MHz, $CDCl_3$) δ (ppm): 159.7, 156.9, 149.5, 141.1, 136.7, 122.3, 120.8, 118.2, 113.8, 70.9, 70.7, 69.8, 67.8. Elem. Anal. Calcd for $C_{40}H_{38}N_4O_5$ • 0.8 AcOEt: C, 71.54; H, 6.17; N, 7.73. Found: C, 71.26; H, 6.20; N, 7.68.

Synthesis of Pt-2 and Pt-1. Compound **2** (500 mg, 0.8 mmol) was dissolved in deaerated acetonitrile (27 mL), and an aqueous solution of K_2PtCl_4 (950 mg, 2.4 mmol in 9 mL water) was added under argon atmosphere. The mixture was heated at reflux under argon for 2 days. After cooling to room temperature and filtration, CH_2Cl_2 was added to the reaction mixture, the organic phase was then separated, dried over $MgSO_4$ and evaporated to dryness in *vacuo*. Compounds **Pt-1** and **Pt-2** were separated by fractional crystallisation in dichloromethane/diethyl ether mixture and obtained as orange powders (**Pt-1**: 55 mg, **Pt-2**: 100 mg). **Pt-2**, Yield: 11%. ^{1}H NMR (400 MHz, CD_2Cl_2) δ (ppm): 9.18 (dd, *J* = 5.6 Hz, $J_{Pt\text{-}H}$ = 44 Hz, 2H, H_6), 7.93 (t, *J* = 7.8 Hz, 4H, H_4), 7.59 (d, *J* = 7.7 Hz, 4H, H_3), 7.29 (d, *J* = 6.3 Hz, 4H, H_5), 7.05 (s, 4H, $H_{2'}$), 4.17 (t, *J* = 4.7 Hz, 4H, H_α), 3.88 (t, *J* = 4.7 Hz, 4H, H_β), 3.76 (m, 8H, H_γ). HR-MS $[M\text{-}Na]^+$ Calculated for $C_{40}H_{36}N_4O_5Cl_2Pt_2Na$: 1135.12507; found: 1135.1236. Elem. Anal. Calcd for $C_{41}H_{39}Cl_2N_4O_5Pt_2$•$Et_2O$: C, 44.93; H, 4.11; N, 4.66. Found: C, 44.99; H, 4.08; N, 4.58. **Pt-1**, Yield: 11%. ^{1}H NMR (400 MHz, CD_2Cl_2) δ (ppm): 9.24 (dd, *J* = 5.6 Hz, $J_{Pt\text{-}H}$ = 44 Hz, 2H, H_6), 7.96 (t, *J* = 7.8 Hz, 2H, H_4), 7.68 (d, *J* = 7.7 Hz, 2H, H_3), 7.30 (d, *J* = 6.3 Hz, 2H, H_5), 7.18 (s, 2H, $H_{2'}$), 4.20 (t, *J* = 4.7 Hz, 2H, CH_2), 3.86 (t, *J* = 4.7 Hz, 2H, CH_2), 3.70 (m, 6H, CH_2), 3.58 (m, 2H, CH_2).

Synthesis of Pt-3. Compound HC≡C-C_6H_4-$O(CH_2CH_2O)_4$-C_6H_4-C≡CH (70 mg, 0.18 mmol) and NaOH (20 mg, 0.5 mmol) were dissolved in MeOH (2 mL) and the mixture was stirred at room temperature for 30 minutes. Then Pt(dpyb)Cl (164 mg, 0.36 mmol) was dissolved in a mixture of MeOH/CH_2Cl_2 (1:1 v/v, 16 mL) and added to the reaction mixture. After stirring for 40 hours, the solvent was removed and the residue was dissolved in CH_2Cl_2. **Pt-3** was precipitated with Et_2O as a yellow powder (105 mg). Yield: 47% yield. ^{1}H NMR (400 MHz, CD_2Cl_2) δ (ppm): 9.49 (m, 4H, H_6), 7.96 (t, *J* = 7.9 Hz, 4H, H_4), 7.72 (d, *J* = 8.2 Hz, 4H, H_3), 7.56 (d, *J* = 7.6 Hz, 4H, $H_{2'}$), 7.48 (d, *J* = 8.7 Hz, 4H, H_{Ar}), 7.26 (m, 6H, $H_{1'}$,H_5), 6.89 (d, *J* = 8.7 Hz, 4H, H_{Ar}), 4.16 (t, *J* = 4.4 Hz, 4H, H_α), 3.87 (t, *J* = 4.8 Hz, 4H, H_β), 3.72 (m, 8H, H_γ,H_δ). ^{13}C NMR (100 MHz, CD_2Cl_2) δ (ppm): 178.7, 169.5, 156.6, 155.3, 143.1, 138.6, 135.0, 132.5, 123.7, 123.5, 122.9, 121.4, 119.4, 114.2, 110.7, 70.8, 70.6, 69.7, 67.5. Elem. Anal. Calcd for $C_{56}H_{46}N_4O_5Pt_2$: C, 54.02; H, 3.72; N, 4.50. Found: C, 53.96; H, 3.70; N, 4.48.

^{1}H NMR studies: To a solution of **Pt-2** (1 mg) in CD_2Cl_2 (0.4 mL) 0.05 mL of a solution of KPF_6 (10 eq.), $NaPF_6$ (10 eq.) or $CsCO_2CH_3$ (10 eq.) in CD_3CN were added. The ^{1}H NMR spectra were recorded before and after each addition. Then, a solution of 10 mg of [18-crown-6] in of CD_2Cl_2 (0.1 mL) was prepared and 0.05 mL of the solution were added to the solution containing **Pt-2** and KPF_6.

Emission studies. A $8.9^{\bullet}10^{-5}$ M solution of **Pt-2** in CH_2Cl_2 was prepared. 3 mL of the solution were degassed and the emission spectrum was recorded. A 10^{-2} M solution of KPF_6 in CH_3CN was prepared and aliquots of 13 µL, corresponding to 0.5 equiv. of KPF_6, or 26 µL, corresponding to 1 equivalent of KPF_6, were added to the degassed solution of Pt-2 under argon. The emission spectrum was recorded after each addition. A 10^{-2} M solution of [18-crown-6] in CH_2Cl_2 was prepared and 520 µL, corresponding to 20 equivalents, were added to the degassed solution of Pt-2 before measuring the emission.

A solution of **Pt-2** in degassed CH_2Cl_2 (10^{-4} M) was first recorded. Then 10 µL of a CH_3CN solution of $NaPF_6$ (5 equiv.) or CH3COOCs (6 equiv.) was added under argon

Photophysical studies

All samples were prepared in HPLC grade solvents with varying concentrations in the order of micromolar. UV-Vis absorption spectra were recorded at room temperature using a Specord 205 UV/Vis/NIR spectrophotometer in quartz cuvettes of 1 cm pathlength. Molar absorptivity determination was verified by linear least-squares fit of values obtained from independent solutions at varying concentrations ranging from 10^{-4} to 10^{-5} M. The sample solutions for the emission spectra were prepared in HPLC grade solvents and degassed via three freeze-pump-thaw cycles. Steady-state luminescence spectra were measured using an Edinburgh FS920 Steady State Fluorimeter combined with a FL920 Fluorescence Lifetime Spectrometer. All samples for steady-state measurements were excited at 400 nm. The spectra were corrected for the wavelength dependence of the detector, and the quoted emission maxima refer to the values after correction. Luminescence quantum yields were determined using $[Ru(bpy)_3]Cl_2$ (Φ = 0.028 in air-equilibrated aqueous solution)[15] as standard. Lifetimes measurements were conducted with 375 nm diode laser excitation (EPL-series).

Methods (theory)

To perform DFT and TD-DFT calculations, we have used the Gaussian program.[16] Our calculations consisted in geometry optimization vibrational spectra determinations and TD-DFT calculations of the different structures. We have applied default procedures, integration grids, algorithms and parameters; except for tighten energy (typically 10^{-10} *a.u.*) and internal forces (10^{-5} *a.u.*) convergence thresholds and the use of the *ultrafine* integration DFT grid. The ground-state geometrical parameters have been determined with the PBE0 functional.[17] The vibrational spectrum has been subsequently determined analytically at the same level of theory and it has been checked that all structures correspond to true minima of the potential energy surface. At least, the first twenty low-lying excited-states have been calculated within the vertical TD-DFT approximation using the same exchange-correlation functional, that is suited for optical spectra of typical dye.[18] Phosphorescence was studied by optimizing the lowest triplet excited-state with unrestricted DFT (PBE0 functional) and determining the frequencies in order to be able to estimate the 0-0 phosphorescence energy that takes into account zero-point vibrational effects. For all our calculations, we used the LanL2DZ atomic basis set for all atoms (and pseudopotential for the metal center), with extra functions on the non-hydrogen atoms: *d* functions of α=0.587, 0.736, 0.961 and 0.648 for C, N, O and Cl, respectively and *f* function of α=0.993 for Pt. During all steps, a modeling of bulk solvent effects (here CH_2Cl_2) through the Polarizable Continuum Model (PCM),[19] using the linear-response approach in its non-equilibrium limit for the TD-DFT part of the calculation. It is important to note that non-covalent interactions are crucial in the present case, and as PBE0 is, as many standard functionals, not ideal to model such effects, we took "dispersion" effects into consideration using the D3-BJ empirical approach.[20] To model the excimers of **Pt-2a** and **Pt-2b**, we first optimized the monomer (**Pt-1)** in its lowest singlet and triplet states, and then added in a previously optimized dimer one complex in its singlet geometry and one complex in its triplet geometry. The contour threshold used to draw all orbitals and spin density are 0.03 and 0.001 au, respectively.

Results and discussion

Synthesis, characterization and photophysical properties

Complexes **Pt-1** and **Pt-2** were prepared as shown in Scheme 2 and characterized using ESI-MS, NMR and elemental analysis (see ESI†, Figures S5 and S6). First, the bis-terdentate pro-ligand **2** was obtained in 46% yield by a Suzuki cross-coupling reaction between compound **1** and 2-(tri-*n*-butylstannyl) pyridine in the presence of $PdCl_2(PPh_3)_2$. Then, complexation of **2** to platinum was achieved upon treatment with K_2PtCl_4 in a CH_3CN:H_2O mixture (3:1 v/v) at 80°C for 48h. We found that the reaction afforded **Pt-2** (11%) together with **Pt-1** (11%) as a side product arising from the cleavage of a C(sp^3)-O bond. The two complexes were isolated as orange compounds after fractional crystallisation in a CH_2Cl_2-Et_2O mixture. Crystals of **Pt-1**, suitable for X-ray analysis, were grown by slow diffusion of diethyl ether into a concentrated CH_2Cl_2 solution and its crystallographic structure is described in Figure 1. Complex **Pt-3** (Scheme 1) was synthesised following a reported procedure[21] through deprotonation of the bis(alkyne) HC≡C-C_6H_4-O(CH_2CH_2O)$_4$-C_6H_4-C≡CH with NaOH in MeOH followed by addition of Pt(dpyb)Cl in CH_2Cl_2 (Scheme S1). Precipitation with Et_2O gave **Pt-3** as a yellow powder in 47% yield, but it decomposed rapidly in solution, this lack of stability can be attributed to the detrimental *trans* effect of the electron-rich alkynyl ligand.

The UV-visible absorption spectra of **Pt-1**, **Pt-2** and **Pt-3** measured in CH_2Cl_2 (298 K) are shown in Figures 2a and S12, respectively, whereas the photophysical data are listed in Table 1. The absorption spectrum of **Pt-1** displays an intense absorption band in the UV region (ranging from 300-350 nm) which can be ascribed to $^1(\pi\text{-}\pi^*)$ transitions of the N^C^N ligand, and a moderately intense band appears at lower-energy from 380 to 450 nm attributed to the typical charge-transfer (CT) transitions.[8]

According to our Time-Dependent Density Functional Theory (TD-DFT) calculations, the first transition to a singlet-excited-state is located at 421 nm and it presents a significant oscillator strength (*f*=0.156) and, together with the second transition at 418 nm (*f*=0.013), it is responsible for the low-energy band observed experimentally for **Pt-1** (see the ESI for details). The first band can be mainly ascribed to a HOMO-LUMO transition, which corresponds to a CT from the metal and the phenyl to the pyridyl moieties, i.e., it presents a mixed MLCT/ILCT character (see Figure S23 in the ESI†). The measured optical absorption spectrum (CH_2Cl_2) of **Pt-2** displays a similar profile with higher molar extinction coefficients, as expected for a "*dimeric*" structure (Figure 2a). For **Pt-2**, we have optimized at the DFT level both the **a** and **b** forms (see Chart 1 and Figure S24 in the ESI†).

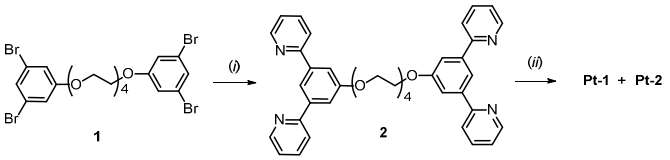

Scheme 2 Reagents and conditions: (*i*) 2-(tri-*n*-butylstannyl)pyridine, LiCl, $PdCl_2(PPh_3)_2$, toluene, reflux, 48h (*ii*) K_2PtCl_4, CH_3CN:H_20 3:1, reflux, 48h.

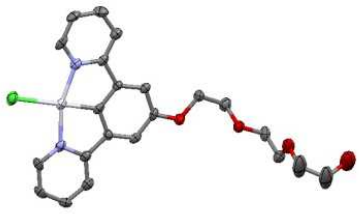

Figure 1 ORTEP diagram of **Pt-1.** Thermal ellipsoids correspond to a 60% probability level

Table 1 Photophysical data in CH_2Cl_2 for complexes **Pt-1**, **Pt-2** and **Pt-3**.

Complex	λ_{abs} / nm ($\varepsilon \times 10^3$ /$M^{-1}cm^{-1}$)[a]	λ_{em}/nm[b]	τ/μs[b]	ϕ %[b,c]
Pt-1	294 (3.5), 379 (0.9), 419 (1.0)	547, 580	11	24
Pt-2	293 (8.5), 379 (2.3), 438 (2.5)	547, 588, 670	1.5[d]	8.7
Pt-3	291 (32.4), 393 (10.9), 450 (4.5)	523, 692	4.1 (25%) 1.2 (75%)[e]	7.4

[a] In CH_2Cl_2 solution (C ≈ 10^{-5} M) at 298 K. [b] In degassed CH_2Cl_2 solution (C ≈ 10^{-5} M) at 298 K, λ_{ex} = 400 nm. [c] $Ru(bpy)_3Cl_2$ as reference. [d] 670 nm. [e] 690 nm.

For the **Pt-2a** conformer the computed spectrum is almost perfectly the double of that of **Pt-1,** *i.e.*, one finds four nearly degenerated transitions at 421 nm (*f*=0.041), 420 nm (*f*=0.253), 418 nm (*f*=0.015) and 418 nm (*f*=0.025), that correspond to a peak centred at 420 nm for a total oscillator strength of 0.334, almost perfectly twice the total *f* of **Pt-1** (0.338). In **Pt-2b**, the Pt-Pt separation is 3.49 Å according to DFT. Compared to **Pt-2a**, the computed absorption spectrum of **Pt-2b** encompasses many more transitions (see the ESI) but the convolution of the TD-DFT states still yields a band centred at ca. 420 nm with a total *f* of 0.308, again similar to the one of a "double" **Pt-1**. Therefore, the absorption spectrum in itself is probably not the best indicator of the form of **Pt-2** in solution: aggregation has a relatively moderate impact on the band shape of the lowest peak. If one compares the total DFT free energies of **Pt-2a** and **Pt-2b**, one obtains that the latter is favoured by 18 kcal.mol^{-1}. To ascertain this value, determined with a rather small basis set, we have also computed the interaction energy in both gas and solvent phases using a single-point calculation made with a very extended atomic basis set, namely *def2*-QZVP. Similar interaction energies were obtained: 21 and 19 kcal.mol^{-1}, respectively. This indicates that the stacked form **Pt-2b** should predominate in solution at the thermal equilibrium at room temperature

For **Pt-3**, we also considered the **a** and **b** conformers during the theoretical calculations (see Figure S24 in the ESI†) and found that the latter is more stable than the former by 17 kcal.mol^{-1} on the free energy scale. In **Pt-3b**, the Pt-Pt separation attains 3.57 Å, quite similar to the value obtained in **Pt-2b**. For the extended conformer, **Pt-3a**, TD-DFT yields absorption that are in the same spectral range as both **Pt-1** and **Pt-2** (though a small redshift is noted), but that are significantly more intense, consistently with the experimental observation (see the ε in Table 1). Indeed, the four lowest singlet transitions being a 455 nm (*f*=0.200), 454 nm (*f*=0.151), 436 nm (*f*=0.058) and 436 nm (*f*=0.077). The frontier orbitals of **Pt-3a** are displayed in Figure S25 in the ESI† and their nature is essentially unmodified compared to **Pt-1**. The spectral properties of the stacked form **Pt-3b**, reveal broader absorption with excited-states located by TD-DFT at 484 nm (*f*=0.003), 462 nm (*f*=0.043), 456 nm (*f*=0.203), 421 nm (*f*=0.008), etc. (see the ESI)

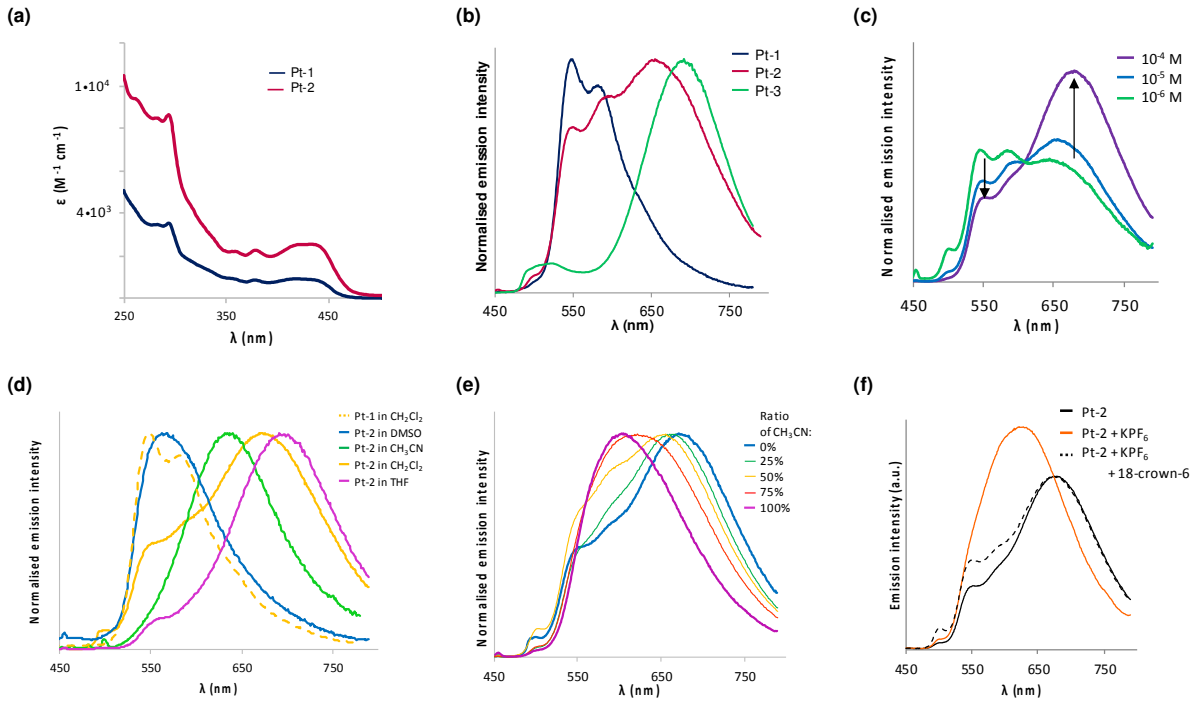

Figure 2 a) UV-vis. absorption spectra of **Pt-1** and **Pt-2** in CH_2Cl_2 solution. b) Emission spectra of **Pt-1**, **Pt-2** and **Pt-3** in CH_2Cl_2 solution (10^{-5} M). c) Emission spectra of **Pt-2** in CH_2Cl_2 at various concentrations. d) Emission spectra of **Pt-2** (conc 10^{-5} M) in various solvents. e) Emission spectra of **Pt-2** in a mixture of CH_2Cl_2 and CH_3CN (10^{-5} M). f) Emission spectra of **Pt-2** in CH_2Cl_2 (8.9 10^{-5}M) (black line), with addition of 5 equiv. of KPF_6 (orange line) and after addition of 18-crown-6 (dashed line).

Nevertheless, the strongest band remains centred at the same position as in **Pt-3a**, confirming that the absorption spectra in themselves are probably not the best indicators of aggregation at the ground-state in the present case.

Complexes **Pt-1**, **Pt-2** and **Pt-3** are luminescent in fluid solution (CH_2Cl_2) at room temperature (see Figure 2b and Table 1). **Pt-1** emits in the green-yellow region of the spectrum displaying a vibrationally resolved spectrum with the first band peaking at 547 nm (CH_2Cl_2, 298 K, λ_{exc} = 400 nm, τ = 11 µs, Φ = 24%). This phosphorescence is attributed to a dominant triplet Ligand-Centered (^{3}LC) excited-state with a small contribution of the metal. Indeed, the emission characteristics compare well with those of the similar complexes.[12] DFT predicts a 0-0 phosphorescence energy at 594 nm and a vertical phosphorescence at 633 nm, corresponding to errors of 0.18 eV and 0.31 eV compared to the experimental values, typical at this level of theory and confirms the ^{3}LC assignment (see Figure S23 in the ESI†). At 10^{-5} M (CH_2Cl_2), the emission spectrum of **Pt-2** (Figure 2b) appears as a very broad band featuring several peaks, and is likely the sum of two electronic transitions, *i.e.*, a monomer-like emission profile for which the maximum is located at 547 nm, and a red-shifted emission band at 670 nm. The assignment of the first is justified by the comparison with the spectrum of the parent complex **Pt-1** which displays a similar emission profile at the same wavelength (Figure 2b) whereas the low-energy band is likely to arise from the formation of an *intra*molecular excimeric excited state, given the very low concentration used. Indeed, this band resembles that of the xanthene-based dinuclear complex xant-(dpybPtCl)$_2$ for which the *intra*molecular excimeric band is centred at 690 nm (CH_2Cl_2, λ_{exc} = 420 nm),[11] as a result of a *rigid* face-face conformation which maximizes the (d-π* or π-π*) interactions between the two organometallic fragments. At 10^{-5} M in CH_2Cl_2, the emission spectrum of complex **Pt-3** appears to be clearly dominated by the excimeric emission (Figure 2b). The spectrum of **Pt-3** is discussed in more details below, but let us first focus on **Pt-2.** Concentration-dependent emissions were recorded for both **Pt-1** and **Pt-2**. When increasing the concentration of **Pt-2** in CH_2Cl_2 solution (from 10^{-6} to 10^{-4} M), the low-energy band progressively becomes more intense at the expense of the short wavelength bands (Figure 2c). Irrespective of the considered concentration, the excitation spectrum closely resembles the corresponding absorption spectral bands of **Pt-2** (Figure S13 in the ESI†). The cause of the red-shifted emission is therefore likely to arise from metal–metal and π-π interactions that are strengthened in the stacked form (**Pt-2b**) when one of the two complexes is in its excited state. As we have seen above, DFT indicates that the chain linking the two complexes is flexible enough to allow interactions between the two Pt(N^C^N) units within the same molecule, (Figure S24 in the ESI†) but at higher concentrations excimeric interactions become significant (Figure 2c). Importantly, for the parent monomer **Pt-1** no evidence of near-IR emission can be found in a 10^{-4} M solution in CH_2Cl_2 (Figure S14 in the ESI†), which suggests that the *intra*molecular interactions significantly dominate in the **Pt-2** excimeric emission, at least in the range of concentration used. In other words, our experiments indicate that the flexible bridge significantly helps in bringing together the two (N^C^N)Pt moieties via a face-to-face configuration for the *intra*molecular association counterbalancing the 4-alkoxy substituent, known to slightly destabilizes these interactions.[8b] Using DFT, we have modelled the "excimer" in both **Pt-2a** and **Pt-2b**, in which one of the two structures is in its (lowest) singlet state and the other in its triplet state. The stabilization of the latter compared to the former attains 21 kcal.mol^{-1}, that is, appears slightly higher than for the corresponding ground-state structure (18 kcal.mol^{-1}, see above). Concomitantly, the separation between the two Pt atoms is slightly smaller in the excimeric form of **Pt-2b** (3.31 Å) than its ground-state counterpart (3.49 Å). For **Pt-2a**, the computed 0-0 phosphorescence wavelength is 565 nm whereas the vertical value is 602 nm. In contrast, for **Pt-2b**, theory predicts 607 nm and 666 nm for the 0-0 and vertical emissions, respectively, illustrating the redshift induced by the stacking. It is nevertheless noticeable that the computed effect is significantly smaller (+64 nm within the vertical approach) than its measured counterpart (ca. +123 nm). The density plots (Figure 3) indicate that as expected the triplet state is purely localized on one moiety in **Pt-2a**, but that in **Pt-2b**, there is a small delocalization on the second complex.

Furthermore, the emission characteristics of **Pt-2** are influenced by the solvent polarity (Figure 2d, Table 2). In a very polar solvent such as DMSO, a broad and unstructured band is observed at 567 nm attributed to the monomer emission with a lower yield. In addition, partial quenching of luminescence occurs -a feature also found for **Pt-3** (see below)- that is attributed to the combination of interaction of the solvent in these square-planar systems, and additional flexibility in the **a** conformers that dominates in DMSO. The photophysical behaviour is very different in THF, where the excimer band prevails, leading to the hallmark red-shifted band (up to 125 nm). One can reasonably assume that the association process is controlled by the nature of the solvent as the result of the amphiphilic nature of **Pt-2** that contains a hydrophobic head - the platinum core Pt(N^C^N)Cl- and a hydrophilic chain.

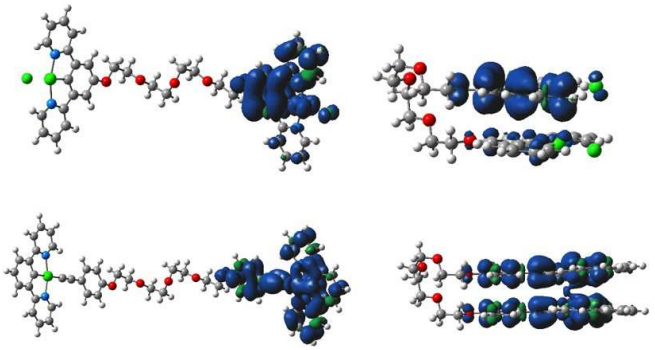

Figure 3 Representation of the spin density difference for the emissive structures of **Pt-2a** (top left), **Pt-2b** (top right), **Pt-3a** (bottom left) and **Pt-3b** (bottom right).

Table 2 Emission data for **Pt-2** and **Pt-3** in various solvents.

	Pt-2		Pt-3	
Solvent	λ_{em}/nm[a]	ϕ_{em} / %[b,c]	λ_{em}/nm[a]	ϕ_{em} / %[b,c]
CH_3CN	632	8.1	489, 520, 684	17
DMSO	567	0.8	531, 678	0.2
THF	692	1.5	493, 526, 700	22

[a] Recorded in degassed solution (10^{-5}M), λ_{ex} = 400 nm. [b] 10^{-5}M; [c] $Ru(bpy)_3Cl_2$ as reference

Significant spectral emission changes are also observed by adding CH_3CN in a CH_2Cl_2 solution (Figure 2e), the spectrum gradually displaying a very broad band structureless centred at 632 nm (10^{-5} M), probably corresponding to the overlap of the two bands for which the monomer emission is predominant, with some contribution of the excimer. These observations show that: (*i*) CH_3CN favours the extended form, and (*ii*) **Pt-2** displays a positive solvatochromism, *i.e.*, a bathochromic shift due to the ILCT character of this 4-alkoxy substituted derivative.[12] At higher concentration (10^{-4} M), the increase of *intra*molecular interactions red-shifts the emission band to 672 nm, which we attribute to a larger intensity in the red-end tail of the spectrum with a concomitant decrease of the proportion relative to the monomer (Figure S15 in the ESI†). In short, the luminescence signatures of **Pt-2** can be easily tuned over the visible part of the spectrum by changing the solvent.

Cation binding can also perturb the interaction process: upon addition of KPF_6 into a CH_2Cl_2 solution of **Pt-2**, the emission spectrum is clearly modified (Figure 2f), leading to a decrease of the low-energy emission band while no modification of the absorption spectrum was observed. It is likely that the binding of K^+, to the oxygen atoms of the linker, significantly reduces or even inhibits the excimer formation.[22] Interestingly, the spectral changes are reversible, addition of [18-crown-6], which is expected to bond K^+ more strongly than **Pt-2**, allows the initial emission spectrum to be recovered (Figure 2f). The ^{1}H NMR spectrum (CD_2Cl_2) of **Pt-2** is also modified when KPF_6 is added. Splitting of all signals with a 1:1 integration ratio occurs, the two Pt moieties become magnetically non equivalent indicating a change at the ground state (Figure S9b in the ESI†). This phenomenon is also reversible upon addition of [18-crown-6] (Figure S9c in the ESI†). Emission studies in the presence $NaPF_6$ leads to similar spectral changes (Figure S16a), showing that cation-binding is not chemoselective. By contrast, the ^{1}H NMR and emission spectra remain unchanged after addition of $CsCO_2CH_3$ (Figures S16b and S10 in the ESI†).

For comparison, we investigated the photophysical properties of the related dinuclear complex **Pt-3** in which the two organometallic moieties are linked by a similar oxyethylene chain but with a different design, *i.e.*, via the ancillary alkynyl ligand (Scheme 1). Photophysical data are compiled in Tables 1 and 2, and selected absorption and photoluminescence spectra are shown in Figures S12 and 2b, respectively. **Pt-3** displays strong luminescence band in CH_2Cl_2, (10^{-5} M) centred at 692 nm, accompanied by a weak structured band at 520 nm. The low-energy band is attributed to the excimer whereas the high-energy band is attributed to a ^{3}LC/LLCT excited state.[22] DFT calculations were performed for both the extended **Pt-3a** in which the two complexes do not interact and **Pt-3b**, in which stacking takes place. The spin density representations of the triplet states are displayed in Figure 3 for both structures. For **Pt-3a**, the emissive state is localized only on one side of the compound, but is significantly more delocalized than in both **Pt-1** and **Pt-2a** (see Figure 3). For this structure, DFT provides a 0-0 phosphorescence at 593 nm, too red-shifted compared to experiment as in **Pt-2a** (see above). What is probably more enlightening is the density difference of **Pt-3b** given in Figure 3. This density shows a full delocalization on the two complexes, contrasting clearly with the case of **Pt-2b**. This result, obtained though the geometry optimization was started with one complex in its ground-state geometry and one in its excited-state (triplet) geometry, clearly hints at a stronger excimeric-like interaction in **Pt-3b** than in **Pt-2b**. Conversely, we computed a 0-0 phosphorescence energy of 663 nm for **Pt-3b**, strongly redshifted compared to **Pt-2b** (607 nm) and the Pt-Pt separation is much smaller in the excimeric form of **Pt-3b** (2.94 Å) than in both the **Pt-2b** excimer (3.31 Å) and the **Pt-3b** ground-state (3.57 Å). The emission of **Pt-3** is also concentration-dependent: increasing the concentration from 10^{-6} to 10^{-4} M yields an increase of the excimer band and a decrease of the monomer emission (Figure S17 in the ESI†). On going from CH_2Cl_2 to CH_3CN or THF, similar emission profiles and luminescence quantum yields were found for **Pt-3** (Table 2 and Figure S18 in the ESI†), hence the emission is not as solvatochromic (except in DMSO) as in **Pt-2**. Notably, complex **Pt-3** has a high propensity to self-assembly, compared to the related mononuclear complex Pt(dpyb)(C≡C-C_6H_5)[23] illustrating again the important role of the linking chain in the excimer formation. Furthermore, by contrast to **Pt-2,** no significant spectroscopic changes were observed upon addition of KPF_6 to a CH_2Cl_2 solution of **Pt-3** (see Figures S11 and S19 in the ESI). These results indicate that **Pt-2** displays a distinctive and unique behaviour for which the change in the nature of the emissive excited states (due to both solvatochromism and, the extended (**a**) and folded (**b**) arrangements) is controlled by solvent polarities.

Notably, in rigid glass at 77 K all N^C^N-complexes **Pt-1**, **Pt-2**, **Pt-3** display exclusively a structured monomer-like emission (see Figures S20-S22 and Table S2 in the ESI†), a feature which contrasts to that of (N^N^N)Pt complexes in which ground-state interactions are stabilized with decrease of temperature leading to red-shifted absorption and emission bands.[7]

Conclusions

In summary, new flexibly-linked dinuclear (N^C^N) platinum complexes have been designed and synthesized. The present work demonstrated the crucial role of the linkage in the formation of excimers in the 4-alkoxy-substituted dpyb-based Pt(II) complexes giving rise to an additional emission band in the near-IR. In particular, our spectroscopic and theoretical investigations have demonstrated that the excimeric

interactions that is very strong in **Pt-3** can be decreased by changing the linker position in **Pt-2**, leading to a compound exhibiting very versatile emissive signatures. Indeed, strategies to regulate the emission colour of **Pt-2** by controlling the noncovalent interactions of luminophores, π-π or/and metal-to-metal interactions, have been achieved by solvent dependence and reversible cation binding. These results demonstrate the peculiar behaviour of N^C^N-platinum(II) complexes compared to terdentate-coordinating (N^N^N) derivatives which display ground-state aggregation properties. These studies should be useful for the better design of deep red-emitters.

Acknowledgements

D.J. acknowledges the *Region des Pays de la Loire* for constant support. This work used computational resources from the CCIPL, the CINES and the local Troy cluster. We thank CNRS for a financial support (PICS CNRS Rennes-Milan) and l'Università Italo Francese (Progetto Galileo 2015/2016; G15_50) for mobility support.

Keywords: platinum • self-assembly • luminescence • time-dependent Density Functional Theory

Notes and references

1 (*a*) J. Kalinowski, V. Fattori, M. Cocchi and J. A. G. Williams, *Coord. Chem. Rev.*, 2011, **255**, 2401–2425; (*b*) A. Y.-Y. Tam and V. W.-W. Yam, *Chem. Soc. Rev.*, 2013, **42**, 1540–1567.

2 (*a*) S.-W. Lai, M. C.-W. Chan, T.-C. Cheung, S.-M. Peng and C.-M. Che, *Inorg. Chem.,* 1999, **38***,* 4046-4055. (*b*) K. M.-C. Wong and V. W.-W. Yam *Coord. Chem. Rev.,* 2007, **251**, 2477-2488; (*c*) V. W.-W. Yam, *Acc. Chem. Res*., 2011, **44**, 424–434.

3 V. W.-W. Yam, V. K.-M. Au and S. Y.-L. Leung, *Chem. Rev.,* 2015, **115**, 7589-7728.

4 (*a*) C.-Hao Tseng, M. A. Fox, J.-L. Liao, C.-H. Ku, Zo.-T. Sie, C-H. Chang, J.-Y. Wang, Z.-N. Chen, G.-H. Leee and Y. Chi, *J. Mater. Chem. C,* 2017, **5**, 1420-1435.

5 (*a*) I. Stengel, C. A. Strassert, L. De Cola, and P. Bäuerle, Chem. Mater. 2011, 23, 3659–3667; (*b*) A. M. Mauro, A. Aliprandi*,* C. Cebrian, D. Wang, C. Kubel, and L. De Cola, *Chem. Commun.,* 2014, **50**, 7269-7272 ; (*c*) A. Aliprandi*,* M. Mauro*,* and L. De Cola*, Nat. Chem.,* 2016*,* **8***,* 10–15. (*d*) S. Sinn, F. Biedermann, and L. De Cola, *Chem. Eur. J.*, 2017, **23**,1965 –1971.

6 (*a*) C. Po, A. Y.-Y. Tam and V. W.-W. Yam, H. L.-K. Fu, *Chem. Sci.,* 2014, **5**, 2688-2695; (*b*) M. H.-Y. Chan, M. Ng, S. Y.-L. Leung, W. H. Lam and V. W.-W. Yam, *J. Am. Chem. Soc.*, 2017, **139**, 8639-8645; (*c*) C. Po, S. Y.-L. Leung and V. W.-W. Yam, *Appl. Mater. Interfaces*, 2017, **9**, 2786−2795 and references therein.

7 (*a*) K. H.-Y. Chan, H.-S. Chow, K. M.-C. Wong, M. C.-L. Yeung and V. W.-W. Yam, *Chem. Sci*., 2010, **1**, 477-482; (*b*) S. Y.-L. Leung, A. Y.-Y. Tam, C.-H. Tao, H. S. Chow and V. W.-W. Yam, *J. Am. Chem. Soc*., 2012, **134**, 1047-1056. *(c*) S. Y.-L. Leung, W. H. Lam and V. W.-W. Yam, *PNAS*, 2013, **110**, 7986-7991; *(d*) X.-S. Xiao, W. Lu and C.-M. Che, *Chem. Sci*., 2014, **5**, 2482-2488.

8 *(a*) J. A. G. Williams, A. Beeby, E. S. Davies, J. A. Weinstein and C. Wilson, *Inorg. Chem*., 2003, **42**, 8609−8611; *(b*) S. J. Farley, D. L. Rochester, A. L. Thompson, J. A. K. Howards and J. A. G. Williams, *Inorg. Chem.,* 2005, **44**, 9690-9703; *(c*) D. L. Rochester, S.Develay, S. Záliš and J. A. G. Williams, *Dalton Trans*., 2009, 1728-1741

9 (*a*) Z. Wang, E. Turner, V. Mahoney, S. Madakuni, T. Groy and J. Li, *Inorg. Chem*., 2010, **49**, 11276-11286; (*b*) Y. Chen, K. Li, W. Lu, S. S.-Y. Chui, C.-W. Ma and C.-M. Che, *Angew. Chem. Int. Ed*., 2009, **48**, 9909-9913; (*c*) W. L. Tong, M. C. W. Chan and S.-M. Yiu, *Organometallics,* 2010, **29**, 6377-6383; (*d*) X. Li, J. Hu, Y. Wu, R. Li, D. Xia, W. Zeng, D. Zhang, Y. Xiang and W. Jin, *Dyes and Pigments,* 2017, **141**, 188-194.

10 (*a*) B. B. W. D'Andrade, J. Brooks, V. Adamovich, M. E. Thompson and S. R. Forrest, *Adv. Mater.*, 2002, **14**, 1032-1036; (*b*) J. Kalinowski, M. Cocchi, D. Virgili, V. Fattori and J. A. G. Williams, *Adv. Mater.* 2007, **19**, 4000-4005; (*c*) W. Mroz, C. Botta, U. Giovanella, E. Rossi, A. Colombo, C. Dragonetti, D. Roberto, R. Ugo, A. Valore and J. A. G. Williams, *J. Mater. Chem.*, 2001, **21**, 8653-8661; (*d*) L. Murphy, P. Brulatti, V. Fattori, M. Cocchi and J. A. G. Williams, *Chem. Commun*. 2012, **48**, 5817-5819; (*e*) J. Kalinowski, M. Cocchi, L. Murphy, J. A. G. Williams and V. Fattori, *Chem. Phys.,* 2010, **378**, 47-57; (*f*) V. N. Kozhevnikov, B. Donnio, B. Heinrich, J. A. G. Williams and D. W. Bruce, *J. Mater. Chem. C,* 2015, **3**, 10177-10187.

11 S. Develay and J. A. G. Williams, *Dalton Trans*., 2008, 4562–4564.

12 A. Colombo, F. Fiorini, D. Septiadi, C. Dragonetti, F. Nisic, A.Valore, D. Roberto, M. Mauro and L. De Cola, *Dalton Trans*., 2015, **44**, 8478-8487.

13 X.-S. Xiao, W. Lu, C.-M. Che, *Chem. Sci*., 2014, **5**, 2482-2488.

14 Y. Liu, A. Kuzuya, R. Sha, J. Guillaume, R. Wang, J. W. Canary, N. C. Seeman, *J. Am. Chem. Soc.*, 2008, **130**, 10882-10883.

15 G. A. Crosby and J. N. Demas, *J. Phys. Chem.*, 1971, ***75***, 991-1024.

16 M. J. Frisch, G. W. Trucks, H. B. Schlegel, G. E. Scuseria, M. A. Robb, J. R. Cheeseman, G. Scalmani, V. Barone, B. Mennucci, G. A. Petersson, H. Nakatsuji, M. Caricato, X. Li, H. P. Hratchian, A. F. Izmaylov, J. Bloino, G. Zheng, J. L. Sonnenberg, M. Hada, M. Ehara, K. Toyota, R. Fukuda, J. Hasegawa, M. Ishida, T. Nakajima, Y. Honda, O. Kitao, H. Nakai, T. Vreven, J. A. Montgomery Jr., J. E. Peralta, F. Ogliaro, M. Bearpark, J. J. Heyd, E. Brothers, K. N. Kudin, V. N. Staroverov, R. Kobayashi, J. Normand, K. Raghavachari, A. Rendell, J. C. Burant, S. S. Iyengar, J. Tomasi, M. Cossi, N. Rega, J. M. Millam, M. Klene, J. E. Knox, J. B. Cross, V. Bakken, C. Adamo, J. Jaramillo, R. Gomperts, R. E. Stratmann, O. Yazyev, A. J. Austin, R. Cammi, C. Pomelli, J. W. Ochterski, R. L. Martin, K. Morokuma, V. G. Zakrzewski, G. A. Voth, P. Salvador, J. J. Dannenberg, S. Dapprich, A. D. Daniels, Ö. Farkas, J. B. Foresman, J. V. Ortiz, J. Cioslowski and D. J. Fox, Gaussian Inc., Wallingford, CT, 2009.

17 C. Adamo and V. Barone, *J. Chem. Phys.*, 1999, **110**, 6158–6170.

18 A. D. Laurent, C. Adamo and D. Jacquemin, *Phys. Chem. Chem. Phys.*, 2014, **16**, 14334–14356.

19 J. Tomasi, B. Mennucci and R. Cammi, *Chem. Rev.*, 2005, **105**, 2999–3094.

20 S. Grimme, S. Ehrlich and L. Goerigk, *J. Comp. Chem*., 2011, **32**, 1456–1465.

21 (*a*) E. Rossi, A. Colombo, C. Dragonetti, D. Roberto, R. Ugo, A. Valore, L. Falciola, P. Brulatti, M. Cocchi and J. A. G. Williams, *J. Mater. Chem*., 2012, **22**, 10650-10655; (*b*) E. Rossi, A. Colombo, C. Dragonetti, S. Righetto, D. Roberto, R. Ugo, A. Valore, J. A. G. Williams, M. G. Lobello, F. De Angelis, S. Fantacci, I. Ledoux-Rak, A. Singh and J. Zyss, *Chem. Eur. J*., 2013, **19**, 9875-9883

22 S. Sinn, F. Biedermann, M. Vishe, A. Aliprandi, C. Besnard, J. Lacour and L. De Cola, *ChemPhysChem,* 2016, **17**, 1829-1834.

23 Y. Chen, K Li, W. Lu, S. S.-Y. Chui, C.-W. Ma, and C.-M. Che, *Angew. Chem. Int. Ed.,* 2009, **48**, 9909-9913

Table of contents

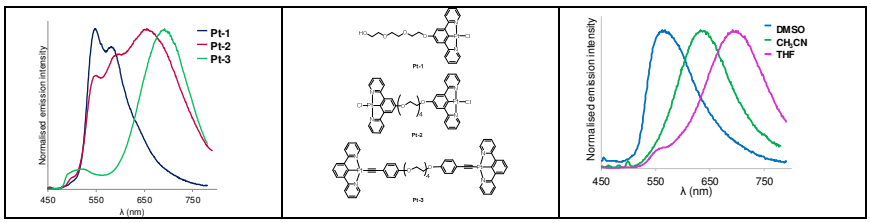

Comparative luminescence studies of the mononuclear complex **Pt-1** and the differently linked dinuclear complexes **Pt-2** and **Pt-3** reveal distinctive luminescent properties. The emission of **Pt-2** can be readily modulated over a wide range of the visible part of the spectrum by changing the solvent that controls the intramolecular interacting processes, i.e., by favouring monomer or excimer emission